

# VR-Based Control of Multi-Copter Operation

Jack T. Hughes, Garegin Mazmanyan, Mohammad Ghufuran, and Hossein Rastgoftar, *Member, IEEE*

**Abstract**—We present a VR-based teleoperation system for multirotor flight that renders a third-person view (TPV) of the vehicle together with a live 3D reconstruction of its surroundings. The system runs on an embedded GPU (Jetson Orin NX) with ROS2/WebXR integration and streams geometry and video to a headset for closed-loop control in previously unmapped spaces. We implement a first-person video (FPV) baseline and perform matched trials with two pilots in unmapped indoor spaces. Quantitative metrics are reported from repeated trials with one pilot ( $N=8$ ). TPV achieved task time comparable to FPV while improving proximal obstacle awareness (minimum obstacle distance +0.20m) and reducing contacts. These results indicate that TPV can preserve control quality while exposing hazards less visible in FPV, supporting safer teleoperation in unknown environments.

**Index Terms**—Human spatial awareness enhancement, human robot interaction, real-time scanning, drone 3D reconstruction, livestreaming.

## I. INTRODUCTION

Although autonomous multi-copter drones have increasingly found real-world applications, human-piloted multi-copters are still widely used in industries such as aerial inspection, photography, and defense. To date, there have been two primary visual input methods provided to pilots: the first is direct line-of-sight operation [1], [2], and the second involves the use of onboard front- or downward-facing cameras [3]. The first method enhances situational awareness by requiring the pilot to maintain unaided visual contact with the aircraft throughout the entire flight, within the Visual Line of Sight (VLOS). As a result, this method limits drone operation to within close proximity of the pilot. In contrast, the second method enables pilots to operate drones beyond the line of sight using onboard cameras. However, it restricts the pilot’s perception to the direction the camera is facing, which reduces situational awareness and can lead to crashes when the drone travels in other directions.

We propose a novel solution that eliminates the major limitations of existing methods. In our system, drone pilots use a virtual reality (VR) headset to view the drone in virtual space from a third-person perspective, as if it were directly in front of them. In addition to the drone itself, a three-dimensional representation of its surroundings is displayed, without requiring any prior knowledge of the drone’s environment.

## II. RELATED WORK

Aerial inspection by multirotor drones has received a lot of attention from many industrial sectors, such as mining [4], [5],

agriculture [6], [7], and construction [8], [9]. Teleoperation is the available tool for controlling multicopters from the ground, where the information collected by onboard sensors can be communicated to a ground station computer. When using such a traditional manual multi-copter control system, the pilot has limited spatial awareness and the ability to communicate control commands to the drone, which means they cannot be adjusted based on in-situ observations the drone gathers. Furthermore, multi-copters’ onboard sensors are usually fixed on the body frame, and therefore, real-time data acquisition quality is significantly affected by the orientation of the aircraft’s body frame, and as a result, the data collected by onboard cameras are not necessarily useful and informative.

Virtual reality (VR) has greatly enhanced human-robot interaction in drone control by providing immersive interfaces that improve spatial awareness. In the context of drones, traditional First-Person View (FPV) systems suffer from limited depth perception, while VR offers more intuitive control. In [10] and [11], it is demonstrated how VR improves maneuverability and control. Refs. [12] and [13] highlight how VR can enhance spatial awareness and human-centered interaction, and [14] shows that using VR aids in operative drones in a complex environment. Recent work on Mixed Reality (MR) interfaces, such as the one designed for omnidirectional aerial vehicles (OMAVs) further enhances the user interaction by allowing operators to control both translational and rotational in six degree freedom [15].

Traditional systems for 3D reconstruction that rely on pre-built maps struggle with real-time updates in dynamic environments. Multi-sensor fusion and real-time SLAM improve adaptability and accuracy in changing environments like urban and off-road [16] [17] [18]. These systems benefit autonomous drones, enabling navigation in unknown spaces, while VR systems rely on real-time mapping for immersive experiences [19] [20] [21].

In drone teleportation, spatial orientation and situational awareness are critical. [12] highlighted that while FPV is immersive, it often limits the operator’s situational awareness by restricting to the drone’s camera field of view. In contrast, third-person view (TPV) systems significantly enhance spatial awareness, providing a broader environmental perspective and superior situational awareness [22] [23]. Study on monoscopic and stereoscopic views shows that TPV improves depth perception, aiding in better control [24].

**Third-person limitations.** Prior work found that third-person viewpoints can degrade navigation performance, reduce spatial orientation, and weaken embodiment in immersive tasks [25]. We consider a different use case, teleoperation of a physical drone. Here TPV complements egocentric cues by revealing lateral and rear hazards that FPV often hides. We therefore evaluate TPV against an FPV baseline and plan a larger study

Authors are with the Aerospace and Mechanical Engineering Department, University of Arizona, Tucson, AZ, 85719 USA email: {jath03, gmazmanyan, ghufuran1942, hrastgoftar}@arizona.edu

to identify when TPV helps and when it hurts.

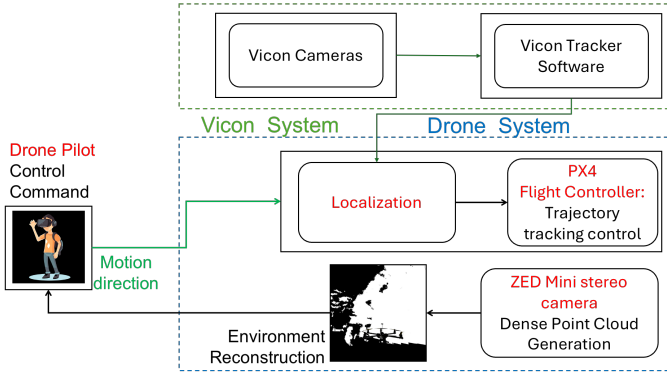


Fig. 1. The architecture proposed for the VR-based perception and control.

### A. Contributions

Existing VR systems for drone teleoperation often rely on static environments and FPV, limiting adaptability and situational awareness and struggling with real-time updates and navigating dynamic, unknown spaces. Our research overcomes these gaps by integrating real-time environment scanning with TPV, enhancing adaptability and spatial awareness for efficient drone operation. In particular, we propose to enhance the spatial awareness of drone by providing virtual reality (VR) capabilities to better sense and control drone operation and interaction. More specifically, we build a novel architecture shown in Fig. 1 for pilot-onboard control of drones using virtual reality to safely operate drones in a constrained environment.

In our work, a multicopter drone with ZED mini stereo cameras is utilized to map the environment in real time, where the drone pilot interprets the mapping and authorizes a proper motion direction command based on a predetermined control scheme. This scheme defines the relationships between the drone pilot and her/his corresponding actions, such as takeoff, landing, hovering, pitch, roll, and yaw maneuvers. The drone's onboard flight controller analyzes the received control signals and adjusts the rotational speed of its motors to perform the desired maneuvers and maintain stable flight.

For our experiment with the VR-Based control system, we want to verify that our system is a viable option for controlling multicopters. To perform this initial experiment, we had a pilot put on the VR headset and, with only our system as visual input, try to fly a multicopter in an unmapped indoor environment towards a wall, stop, return to the starting position, and land safely. This simple test can demonstrate three important points. First, it shows that the system provides enough visual feedback about the multicopter's position and orientation in space to fly it in a controlled manner. Second, it shows that the system's latency is low enough that the pilot can react to the multicopter's movement accordingly. Third, it shows that an unknown environment can be mapped and displayed to the pilot in real time.

## III. SYSTEM

Our system includes a hexacopter, a human operator, and Meta Quest 3 for establishing interaction between the human and hexacopter. The hexacopter model and control are presented in III-A and III-B, respectively, followed by the description of the VR system in Section III-C.

### A. Hexacopter Model

To localize the hexacopter motion, we define a global coordinate system that is fixed on the ground with orthonormal base vectors  $\hat{\mathbf{e}}_1$ ,  $\hat{\mathbf{e}}_2$ , and  $\hat{\mathbf{e}}_3$ . We also define a local (body) coordinate system that is fixed on the hexacopter body, with orthonormal base vectors  $\hat{\mathbf{c}}_1$ ,  $\hat{\mathbf{c}}_2$ , and  $\hat{\mathbf{c}}_3$ . We can use the 3-2-1 Euler angle standard to characterize the orientation of the hexacopter at any time, where we use  $\phi$ ,  $\theta$ , and  $\psi$  to denote the hexacopter's roll, pitch, and yaw angles, respectively. The angular velocity of the hexacopter is expressed with respect to the body coordinate system by

$$\boldsymbol{\Omega} = p\hat{\mathbf{c}}_1 + q\hat{\mathbf{c}}_2 + r\hat{\mathbf{c}}_3 \quad (1)$$

where  $p$ ,  $q$ , and  $r$  are the angular velocity components when it is expressed with respect to the body coordinate system and obtained based on  $\phi$ ,  $\theta$ ,  $\psi$ ,  $\dot{\phi}$ ,  $\dot{\theta}$ , and  $\dot{\psi}$  by

$$\begin{bmatrix} p \\ q \\ r \end{bmatrix} = \begin{bmatrix} 1 & 0 & \sin\theta \\ 0 & \cos\phi & \cos\theta\sin\phi \\ 0 & -\sin\phi & \cos\phi\cos\theta \end{bmatrix} \quad (2)$$

The equation of motion of a hexacopter with mass  $m$  and mass moment of inertia tensor  $\mathbf{J}$  is obtained by

$$m\ddot{\mathbf{r}} = -mg\mathbf{e}_3 + f\hat{\mathbf{c}}_3, \quad (3a)$$

$$\mathbf{J}\dot{\boldsymbol{\Omega}} + \boldsymbol{\Omega} \times \mathbf{J}\boldsymbol{\Omega} = \mathbf{T} \quad (3b)$$

where  $\mathbf{r}$  is the position of the hexacopter measured with respect to the inertial coordinate system,  $f$  is the magnitude of the thrust force generated by all six rotors, and  $\mathbf{T}$  is control torque.

### B. Controller

The hexacopter applies the cascaded position and attitude controllers. The position controller aim to generate desired force

$$\mathbf{F}_{des} = -\mathbf{K}_p(\dot{\mathbf{r}} - \dot{\mathbf{r}}_T) - \mathbf{K}_v(\mathbf{r} - \mathbf{r}_T) + mg\hat{\mathbf{c}}_3 + m\ddot{\mathbf{r}}_T, \quad (4)$$

where  $\mathbf{r}_T$  and  $\dot{\mathbf{r}}_T$  are the commanded position and velocity, and  $\mathbf{K}_p$  and  $\mathbf{K}_v$  are positive definite gain matrices. By projecting  $\mathbf{F}_{des}$  onto  $\hat{\mathbf{c}}_3$ , the desired thrust force is denoted by  $f_{des}$  and obtained by

$$f_{des} = \mathbf{F}_{des} \cdot \hat{\mathbf{c}}_3, \quad (5)$$

By knowing  $\mathbf{F}_{des}$ , the desired orientations of the body base vectors are denoted by  $\hat{\mathbf{c}}_{1,des}$ ,  $\hat{\mathbf{c}}_{2,des}$ , and  $\hat{\mathbf{c}}_{3,des}$ , and obtained by

$$\hat{\mathbf{c}}_{3,des} = \frac{\mathbf{F}_{des}}{\|\mathbf{F}_{des}\|}. \quad (6a)$$

$$\hat{\mathbf{c}}_{1,des} = \frac{(\hat{\mathbf{e}}_3 \times \hat{\mathbf{h}}) \times \hat{\mathbf{c}}_{3,des}}{\|(\hat{\mathbf{e}}_3 \times \hat{\mathbf{h}}) \times \hat{\mathbf{c}}_{3,des}\|}, \quad (6b)$$

$$\hat{\mathbf{c}}_{2,des} = \hat{\mathbf{c}}_{3,des} \times \hat{\mathbf{c}}_{1,des}. \quad (6c)$$

where

$$\hat{\mathbf{h}} = \frac{(\hat{\mathbf{c}}_1 \cdot \hat{\mathbf{e}}_1)\hat{\mathbf{e}}_1 + (\hat{\mathbf{c}}_1 \cdot \hat{\mathbf{e}}_2)\hat{\mathbf{e}}_2}{\|(\hat{\mathbf{c}}_1 \cdot \hat{\mathbf{e}}_1)\hat{\mathbf{e}}_1 + (\hat{\mathbf{c}}_1 \cdot \hat{\mathbf{e}}_2)\hat{\mathbf{e}}_2\|}. \quad (7)$$

is the heading vector. By knowing  $\hat{\mathbf{c}}_{1,des}$ ,  $\hat{\mathbf{c}}_{2,des}$ , and  $\hat{\mathbf{c}}_{3,des}$ , we obtain desired rotation matrix

$$\mathbf{S}_{des} = [\hat{\mathbf{c}}_{1,des} \quad \hat{\mathbf{c}}_{2,des} \quad \hat{\mathbf{c}}_{3,des}] \quad (8)$$

We also define rotation matrix

$$\mathbf{S} = [\hat{\mathbf{c}}_1 \quad \hat{\mathbf{c}}_2 \quad \hat{\mathbf{c}}_3] \quad (9)$$

and compute attitude error as follows:

$$\mathbf{e}_R = \frac{1}{2} (\mathbf{S}_{des}^T \mathbf{S} - \mathbf{S}^T \mathbf{S}_{des})^\vee. \quad (10)$$

where  $\square^\vee$  is the vee map which transforms a skew-symmetric matrix into a vector by

$$\begin{bmatrix} 0 & a & b \\ -a & 0 & c \\ -b & -c & 0 \end{bmatrix}^\vee = \begin{bmatrix} -c \\ b \\ -a \end{bmatrix}, \quad \forall (a, b, c) \in \mathbb{R}^3. \quad (11)$$

We denote the desired torque that needs to be generated by the hexacopter rotors by  $\mathbf{T}_{des}$  and compute it by

$$\mathbf{T}_{des} = -\mathbf{K}_R \mathbf{e}_R - \mathbf{K}_\omega \mathbf{e}_\omega, \quad (12)$$

where  $\mathbf{K}_R$  and  $\mathbf{K}_\omega$  are diagonal gain matrices, and

$$\mathbf{e}_\omega = \boldsymbol{\Omega} - \boldsymbol{\Omega}_T. \quad (13)$$

Note that  $\boldsymbol{\Omega}_T$  is the target angular velocity.

### C. Meta Quest 3

Our system uses a Meta Quest 3 to render and display the virtual environment. The rendering is done in a WebXR-based website through Three.js and is hosted on the onboard Jetson computer. This enables the system to be used on any VR headset that supports WebXR and even allows for multiple simultaneous users. The headset is connected to ROS2 through `rosbridge_server`, as shown in Fig. 5.

The virtual environment uses the coordinate system created by the ZED camera, where the starting point of the camera, and thus the multi-copter, is used as the origin and the environment is placed relative to that point. Before rendering, this coordinate system is shifted 5 meters in front of the pilot so that the pilot sees the multi-copter and environment in front of them instead of being co-located.

## IV. EXPERIMENTAL SETUP

The experiment is conducted in a robotic facility equipped with 17 Vicon Valkyrie cameras and a Vicon tracking system offering high-resolution tracking system within a  $30\text{m} \times 15\text{m} \times 5\text{m}$  indoor testing facility.



Fig. 2. The hexacopter used for the experiment.

### A. Hardware Setup

For the experimental validation of our proposed approach, we are utilizing a hexacopter (Fig. 2) equipped with Nvidia Jetson Orin NX 16GB (Table I) and SeteroLabs ZED X Mini Camera (Table II). The Camera is connected to Jetson using a ZED GMSL2 capture card, which processes the camera image using the Jetson GPU. The Jetson and the camera are powered by a 4-cell Lithium Polymer battery, with a voltage regulator stepping down the voltage from 16.8V to 12V to ensure stable power delivery.

TABLE I  
NVIDIA JETSON SPECIFICATIONS

Parameter	Description
GPU	1024-core NVIDIA Ampere GPU with 32 Tensor Cores
CPU	8-core Arm@ Cortex@-A78AE v8.2 64-bit
Memory	16GB 128-bit LPDDR5
Storage	128 GB ssd

Our flight controller of choice is the Pixhawk 6C mini, paired with a Flysky radio for remote control and communication. To provide external pose data for flight, we use the Vicon motion capture system, which increases positional accuracy. We designed and 3D-printed custom mounts for both the Jetson and the camera to integrate them securely into the drone's frame.

TABLE II  
CAMERA SPECIFICATION

Parameter	Description
Camera Resolution	600p at 60 FPS
Field of View (FOV)	110 (H) x 80 (V) x 120° (D) max
Depth Range	0.1m to 8m (0.3ft to 26ft)
Dimensions	94 x 32 x 37 mm (3.69 x 1.25 x 1.44 in)
Baseline	5 cm (1.97 in)
Weight	150 g (0.33 lb)

For user interaction and control, Mixed Reality (MR) provides intuitive holographic controls, enhancing situational awareness, and user studies confirm the effectiveness of MR controls across various experience levels [15]. For the mixed reality (MR) component, we are using Meta Quest 3 (Fig 3) due to its cutting-edge features, such as high-resolution displays, standalone functionality, and mixed realities capabilities. Control is achieved using the included Meta Quest Touch Plus controllers.

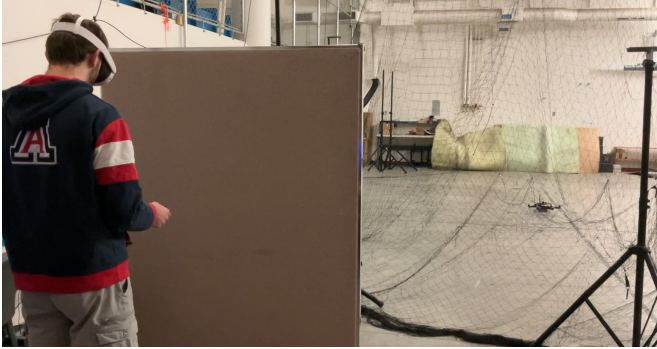


Fig. 3. Operator with Meta Quest 3

### B. Software Setup

Figure 5 illustrates our software architecture. Three.js is used for rendering the VR scene on the front-end, which is done onboard the headset to minimize latency. There are three main communication channels between the back-end and front-end: ROS2 communication, a websocket for mesh data, and a WebRTC video stream. Most data, including control signals from the user and tracking data from the camera, are sent over ROS2 via the rosbridge suite. We determined that sending the mesh data over ROS2 resulted in significantly reduced performance due to the need to serialize and deserialize the large mesh structures to and from ROS2 messages. For this reason, the mesh data is sent in a custom binary format that minimizes serialization and deserialization costs. Additionally, WebRTC is used to send a video stream because it is a low latency, low bandwidth solution.

To demonstrate the possibility of controlling the hexacopter exclusively over the WiFi connection using our system, a simple control scheme was implemented for the standard VR controllers included with the Quest 3 headset. Pilots can interact with the right-hand joystick to control the velocity of the hexacopter in any direction in the XY plane. For example, when the joystick is pushed upward, the hexacopter will move at a constant velocity in the forward direction.

An important statistic when evaluating a system’s capability for real-time use is latency. For example [26] concludes that the latency threshold to be perceived as real time is significantly below 100 ms, and their experiments found that the median latency perception threshold is 54 ms.

**Latency measurement.** At each frame, the VR server publishes a timestamped `PoseStamped` on `/vrserver/tracking`. The client echoes the most recent message back on `/vrserver/tracking_echo`.

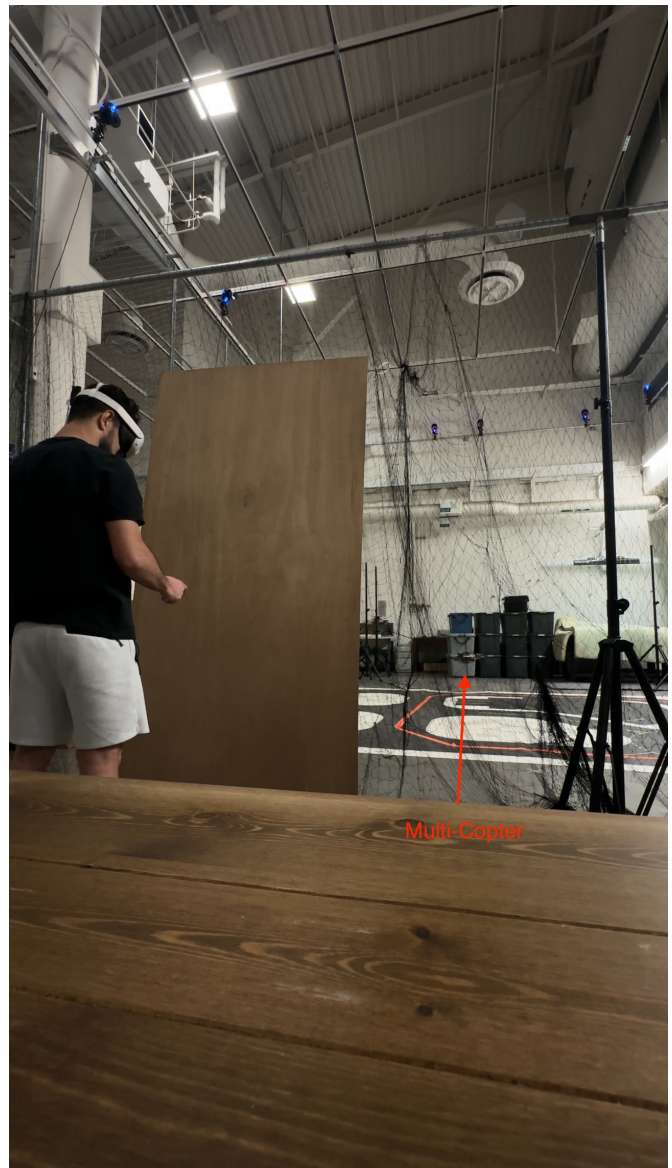


Fig. 4. Second pilot conducting VR teleoperation with the Meta Quest 3 inside the safety enclosure (TPV/FPV trials).

We compute round-trip time (RTT) between transmit and echo receipt and report a one-way estimate as  $RTT/2$ . Rendering on the headset is small relative to transport and treated as negligible. One-way statistics (median, mean, P95, max, and fraction  $> 100$  ms) are computed offline from the echo logs for pre/post comparisons.

The software is all deployed on a Nvidia Jetson Orin NX. It is configured to launch the software at boot using a systemd service that runs a ROS2 launch file, and offers the following advantages:

- 1) Portability and flexibility, WebXR works on any compatible headset.
- 2) Bandwidth utilization, compressed video and a binary mesh format reduce load.
- 3) Security, transport is encrypted with TLS.

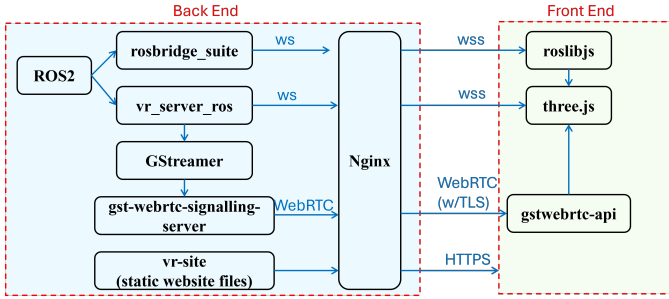


Fig. 5. Functionality of software setup.

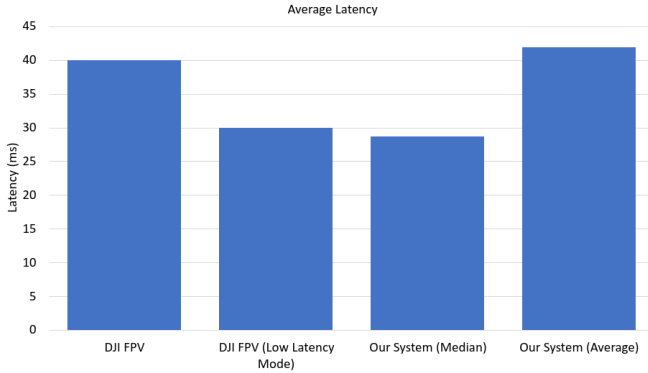


Fig. 6. Comparison of latency with commercial offering.

### C. Robustness and Operational Fallbacks

**Manual mapping throttle.** When transient load increases, the operator can disable mapping using the built-in toggle (ROS2 service `/vrserver/mapping`, controller `select`). In this mode, only pose and video are streamed.

**FPV-only fallback.** If persistent congestion or mapping load impairs readability, the client can run in FPV mode by launching the page with `?mode=fpv`. This shows a full-screen video feed while still rendering vehicle pose.

**State indicators.** The backend publishes tracking and mapping state on `/vrserver/status`; the front end surfaces status cues. **Operator SOP.** If one-way latency exceeds about 100 ms or state is non-OK for more than about 2 s, the sequence is: disable mapping, if needed switch to FPV, then re-enable mapping once stable.

### D. Limitations

Our current evaluation is constrained to an indoor flight volume because the pose backbone relies on a Vicon motion-capture system. This infrastructure provides high-rate, high-accuracy ground truth but precludes outdoor trials, where GNSS availability, wind, lighting variability, and larger operational baselines may affect mapping quality and link behavior. The laboratory is a controlled facility with restricted access, which limits the participant pool. Two trained pilots flew the protocol. The sample size is small, so results should be interpreted as evidence of technical feasibility in controlled conditions rather than population-level usability. Future work

TABLE III  
TPV vs FPV (SINGLE PILOT, REPEATED TRIALS; REPORTED METRICS)

Condition	Time (s)	Min Dist (m)	Contacts	Smoothness
FPV	55±6	0.62	1/4	baseline
TPV	57±7	0.82	0/4	within 5%

TABLE IV  
ONE-WAY TRACKING LATENCY (MS), BEFORE VS. AFTER OPTIMIZATIONS

Condition	Median	Mean	P95	Max	%>100
Pre-opt (full)	28.7	41.9	105.0	507.0	6.0
Post-opt (full)	16.1	29.8	86.0	497.4	3.16
Post-opt (steady-state)	15.9	24.2	74.6	246.4	1.47

will migrate to a VIO+GNSS/RTK outdoor stack and conduct an IRB-approved multi-participant study in open test ranges.

The system relies on the ZED camera and accompanying SDK for all simultaneous localization and mapping (SLAM) tasks, which limits the quality of the rendered environment to the quality that the ZED SDK can produce. Real-time SLAM is a field that is rapidly advancing and future progress in that field will directly translate to an improved experience using systems such as this one as environment maps get more detailed. Performance improvements in SLAM implementations will also lead to a significantly improved user experience because SLAM is the most compute-intensive task the system performs, and thus the main performance limitation.

## V. EXPERIMENTAL RESULTS

Two trained pilots completed the protocol. We evaluated TPV (third-person VR with live mapping) and an FPV baseline (video-only). Each pilot executed: takeoff → approach a wall and stop at commanded standoff  $[d_{cmd}]$  → return → land. For quantitative analysis we report repeated trials from one pilot ( $N=8$ ) to control within-subject variability.

**Metrics.** We logged task time, minimum obstacle distance, contacts, path length, and velocity smoothness (acceleration  $\ell_2$ ). Latency was measured via timestamped ROS2 pings echoed from the headset, yielding one-way estimates (median, mean, P95, max, and fraction > 100 ms).

**TPV vs FPV Performance.** Table III summarizes performance. Task time was comparable (FPV 55±6 s vs TPV 57±7 s). Minimum obstacle distance improved in TPV (FPV 0.62 m → TPV 0.82 m, +0.20 m), and contacts were lower (FPV 1/4 vs TPV 0/4). Path length and smoothness differed by < 5%.

### A. Latency after Optimizations

Using the timestamped echo method, the *post-optimization one-way latency* for the full run is: median **16.1** ms, mean **29.8** ms, P95 **86.0** ms, max **497.4** ms, and **3.16%** > 100 ms. Because the largest excursions occur at startup and at a terminal PX4 emergency stop, we also report a steady-state slice excluding the first 10 s and frames > 250 ms: median **15.9** ms, mean **24.2** ms, P95 **74.6** ms, max **246.4** ms, and **1.47%** > 100 ms.

**Context vs Commercial Latency** As in Fig. 6, the post-optimization median remains below commonly cited real-time

## Tracking Latency over Time

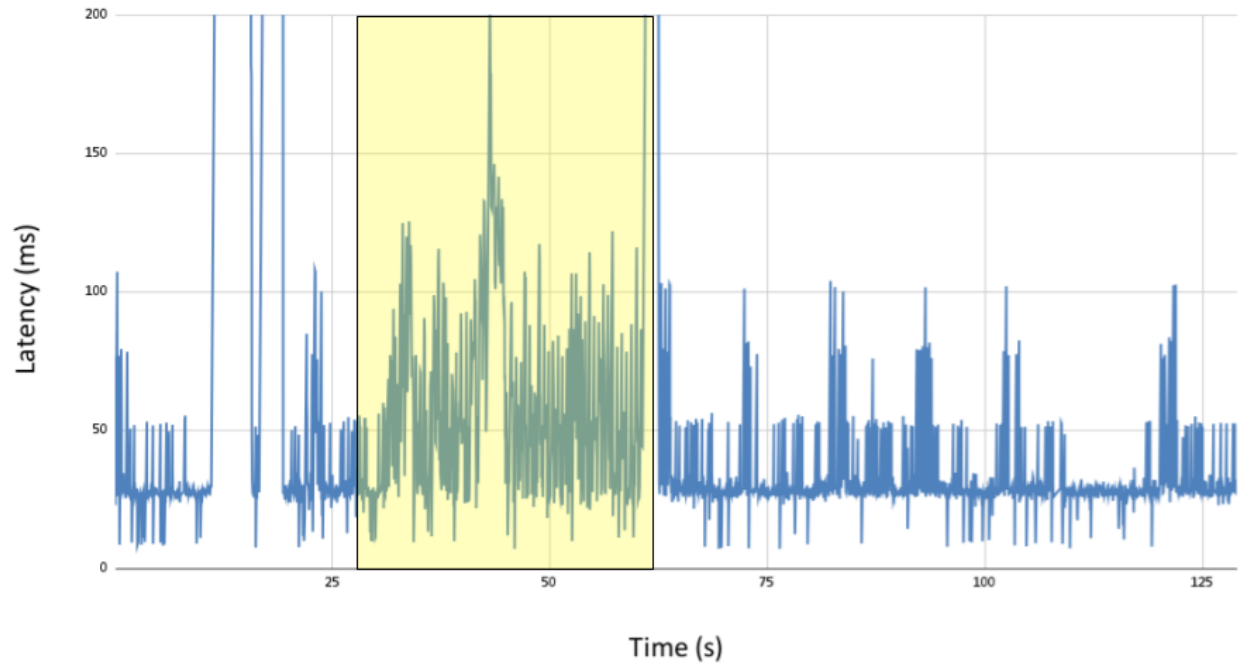


Fig. 7. One-way tracking latency over time estimated as  $RTT/2$ . The shaded interval marks a sustained mapping burst where variance rises. The two highest excursions occur at system startup and at a terminal emergency stop issued via the PX4 controller at the end of the flight. Operators can pause mapping or switch to FPV when tail latency grows (see Table IV).

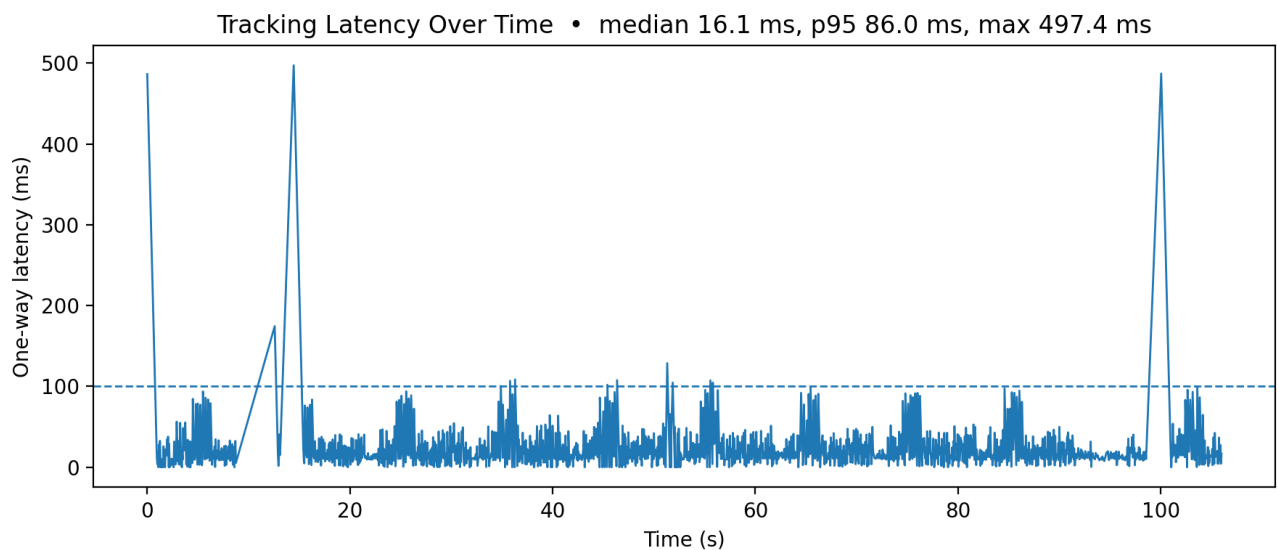


Fig. 8. Post-optimization one-way tracking latency over time ( $RTT/2$ ). Dashed line shows 100 ms. Full run: median **16.1** ms, mean **29.8** ms, P95 **86.0** ms, max **497.4** ms, and **3.16%** of frames > 100 ms. Steady state, excluding the first 10 s and frames > 250 ms: median **15.9** ms, mean **24.2** ms, P95 **74.6** ms, max **246.4** ms, and **1.47%** > 100 ms. The two largest spikes are attributable to system startup and a terminal PX4 emergency stop; neither reflects steady-state operation.

perception thresholds (Fig. 9) and comparable to commercial FPV offerings, while P95 and tail behavior improve when mapping bursts are avoided.

## VI. CONCLUSION

These results show that our system is a viable option for improving the spatial awareness of multi-copter pilots in an unknown environment. The virtual environment, while rough,

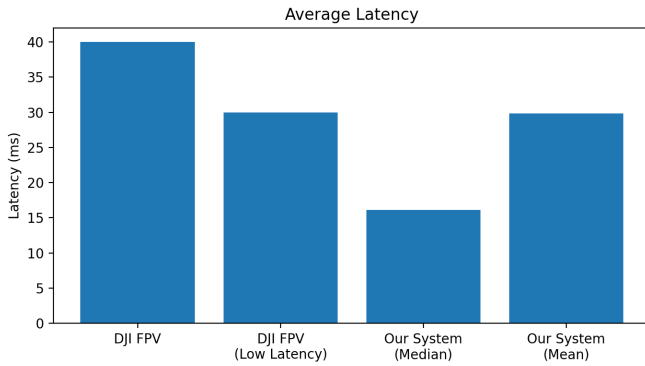
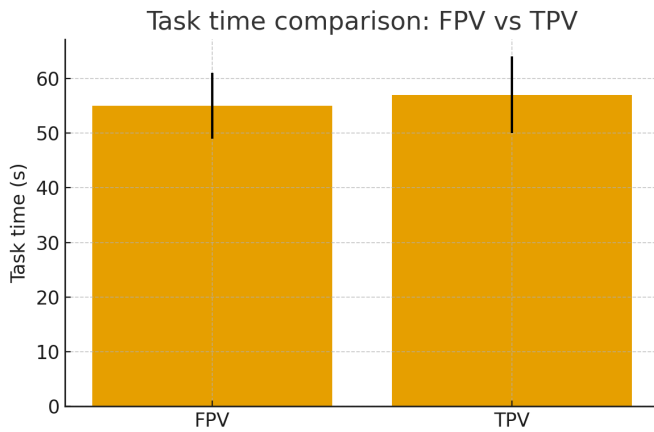
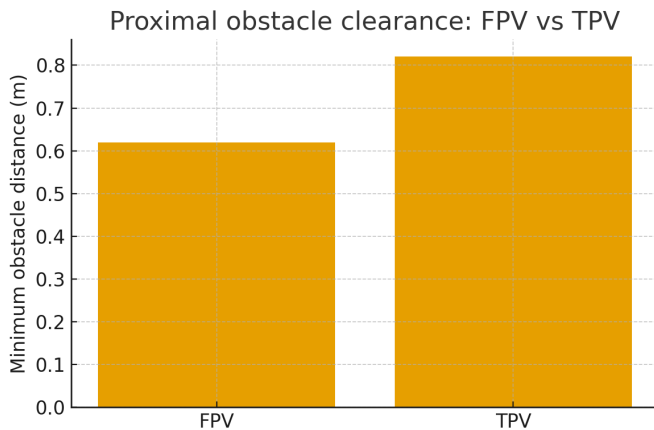


Fig. 9. Post-optimization latency summary. Full run: median **16.1 ms**, mean **29.8 ms**, P95 **86.0 ms**, max **497.4 ms**, and **3.16%** > 100 ms. Steady state, excluding first 10 s and frames > 250 ms: median **15.9 ms**, mean **24.2 ms**, P95 **74.6 ms**, max **246.4 ms**, and **1.47%** > 100 ms.



(a) Task time



(b) Minimum obstacle distance

Fig. 10. FPV vs TPV performance in matched trials. Top, task time: FPV  $55 \pm 6$  s, TPV  $57 \pm 7$  s. Bottom, minimum distance: FPV 0.62 m, TPV 0.82 m.

adequately informs pilots of nearby obstacles in a way that FPV cameras cannot. The virtual drone mimics the movement of the real drone with a low enough latency for pilots to receive real-time visual feedback.

Additionally, we have demonstrated that control can be achieved using VR controllers, sending control signals over

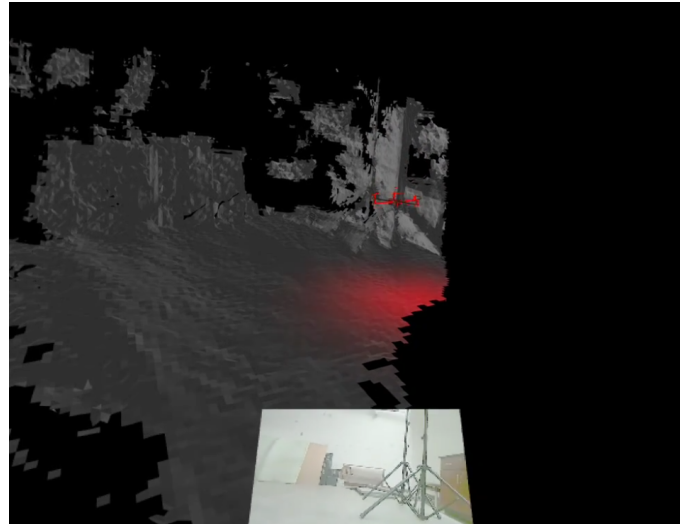


Fig. 11. Screenshot of partially reconstructed environment, hexacopter, and video stream.



Fig. 12. FPV camera stream rendered in the VR client. FPV-only fallback prioritizes the video feed while maintaining pose cues.

WiFi. This opens the door for fully remote operation of multi-copters with minimal loss in environmental awareness.

Other future work may include investigating alternative VR-based control options such as gestures, including additional cameras to map more of the environment at once, and attempting to add camera images as a texture on the rendered mesh to provide more detail about the environment.

## VII. ACKNOWLEDGEMENT

This work was supported by the National Science Foundation under Award 2133690 and Award 1914581.

## REFERENCES

- [1] Y. Han, J. Wei, and A. Yilmaz, "Uas navigation in the real world using visual observation," in *2022 IEEE Sensors*. IEEE, 2022, pp. 1–4.

- [2] A. Hobbs and B. Lyall, "Human factors guidelines for unmanned aircraft systems," *Ergonomics in Design*, vol. 24, no. 3, pp. 23–28, 2016.
- [3] R. Sato, E. M. Badard, C. S. Romulo, T. Wada, and A. Ming, "Development of an aerial manipulation system using onboard cameras and a multi-fingered robotic hand with proximity sensors," *Sensors*, vol. 25, no. 2, p. 470, 2025.
- [4] V. Holuša, F. Beneš, and M. Vaněk, "Utilization of augmented and virtual reality in geoscience," *GeoScience Engineering*, vol. 68, no. 1, pp. 22–32, 2022.
- [5] A. Kamran-Pishhesari, A. Moniri-Morad, and J. Sattarvand, "Applications of 3d reconstruction in virtual reality-based teleoperation: A review in the mining industry," *Technologies*, vol. 12, no. 3, p. 40, 2024.
- [6] M. E. de Oliveira and C. G. Corêa, "Virtual reality and augmented reality applications in agriculture: a literature review," in *2020 22nd symposium on virtual and augmented reality (svr)*. IEEE, 2020, pp. 1–9.
- [7] J. Huuskonen and T. Oksanen, "Soil sampling with drones and augmented reality in precision agriculture," *Computers and electronics in agriculture*, vol. 154, pp. 25–35, 2018.
- [8] J.-Y. Cheng, E. Lunardini Silva Mendes, M. Gheisari, and I. Jeelani, "Construction worker-drone safety training in a 360 virtual reality environment: A pilot study," *EPiC Series in Built Environment*, vol. 3, 2022.
- [9] G. Albeaino, R. Eiris, M. Gheisari, and R. R. Issa, "Dronesim: A vr-based flight training simulator for drone-mediated building inspections," *Construction Innovation*, vol. 22, no. 4, pp. 831–848, 2022.
- [10] H. Stedman, B. B. Kocer, M. Kovac, and V. M. Pawar, "Vrtabmap: A configurable immersive teleoperation framework with online 3d reconstruction," in *2022 IEEE International Symposium on Mixed and Augmented Reality Adjunct (ISMAR-Adjunct)*, 2022, pp. 104–110.
- [11] Y. Luo, J. Wang, Y. Pan, S. Luo, P. Irani, and H.-N. Liang, "Teleoperation of a fast omnidirectional unmanned ground vehicle in the cyber-physical world via a vr interface," in *Proceedings of the 18th ACM SIGGRAPH International Conference on Virtual-Reality Continuum and Its Applications in Industry*, ser. VRCAI '22. New York, NY, USA: Association for Computing Machinery, 2023. [Online]. Available: <https://doi.org/10.1145/3574131.3574432>
- [12] B. B. Kocer, H. Stedman, P. Kulik, I. Caves, N. Van Zalk, V. M. Pawar, and M. Kovac, "Immersive view and interface design for teleoperated aerial manipulation," in *2022 IEEE/RSJ International Conference on Intelligent Robots and Systems (IROS)*, 2022, pp. 4919–4926.
- [13] C. Liu and S. Shen, "An augmented reality interaction interface for autonomous drone," in *2020 IEEE/RSJ International Conference on Intelligent Robots and Systems (IROS)*, 2020, pp. 11419–11424.
- [14] Y. Chen, B. Zhang, J. Zhou, and K. Wang, "Real-time 3d unstructured environment reconstruction utilizing vr and kinect-based immersive teleoperation for agricultural field robots," *Computers and Electronics in Agriculture*, vol. 175, p. 105579, 2020. [Online]. Available: <https://www.sciencedirect.com/science/article/pii/S0168169920311479>
- [15] M. Allenspach, T. Kötter, R. Bähnemann, M. Tognon, and R. Siegwart, "Design and evaluation of a mixed reality-based human-robot interface for teleoperation of omnidirectional aerial vehicles," in *2023 International Conference on Unmanned Aircraft Systems (ICUAS)*, 2023, pp. 1168–1174.
- [16] Q. Li, J. P. n. Queralta, T. N. Gia, Z. Zou, and T. Westerlund, "Multi-sensor fusion for navigation and mapping in autonomous vehicles: Accurate localization in urban environments," *Unmanned Systems*, vol. 08, no. 03, pp. 229–237, 2020. [Online]. Available: <https://doi.org/10.1142/S2301385020500168>
- [17] A. Chalvatzaras, I. Pratikakis, and A. A. Amanatiadis, "A survey on map-based localization techniques for autonomous vehicles," *IEEE Transactions on Intelligent Vehicles*, vol. 8, no. 2, pp. 1574–1596, 2023.
- [18] M. Zhao, X. Guo, L. Song, B. Qin, X. Shi, G. H. Lee, and G. Sun, "A general framework for lifelong localization and mapping in changing environment," in *2021 IEEE/RSJ International Conference on Intelligent Robots and Systems (IROS)*, 2021, pp. 3305–3312.
- [19] W. Liu, W. Sun, and Y. Liu, "Dloam: Real-time and robust lidar slam system based on cnn in dynamic urban environments," *IEEE Open Journal of Intelligent Transportation Systems*, pp. 1–1, 2021.
- [20] Q. Zou, Q. Sun, L. Chen, B. Nie, and Q. Li, "A comparative analysis of lidar slam-based indoor navigation for autonomous vehicles," *IEEE Transactions on Intelligent Transportation Systems*, vol. 23, no. 7, pp. 6907–6921, 2022.
- [21] L. Wijayathunga, A. Rassau, and D. Chai, "Challenges and solutions for autonomous ground robot scene understanding and navigation in unstructured outdoor environments: A review," *Applied Sciences*, vol. 13, no. 17, 2023. [Online]. Available: <https://www.mdpi.com/2076-3417/13/17/9877>
- [22] M. Inoue, K. Takashima, K. Fujita, and Y. Kitamura, "Birdviewer: Surroundings-aware remote drone piloting using an augmented third-person perspective," in *Proceedings of the 2023 CHI Conference on Human Factors in Computing Systems*, ser. CHI '23. New York, NY, USA: Association for Computing Machinery, 2023. [Online]. Available: <https://doi.org/10.1145/3544548.3580681>
- [23] R. Temma, K. Takashima, K. Fujita, K. Sueda, and Y. Kitamura, "Third-person piloting: Increasing situational awareness using a spatially coupled second drone," 10 2019, pp. 507–519.
- [24] J. J. Roldán, E. Peña-Tapia, A. Martín-Barrio, M. A. Olivares-Méndez, J. Del Cerro, and A. Barrientos, "Multi-robot interfaces and operator situational awareness: Study of the impact of immersion and prediction," *Sensors*, vol. 17, no. 8, 2017. [Online]. Available: <https://www.mdpi.com/1424-8220/17/8/1720>
- [25] D. Medeiros, R. K. dos Anjos, D. Mendes, J. M. Pereira, A. Raposo, and J. A. Jorge, "Keep my head on my shoulders!: Why third-person is bad for navigation in VR," in *Proceedings of the 24th ACM Symposium on Virtual Reality Software and Technology (VRST '18)*. New York, NY, USA: Association for Computing Machinery, 2018.
- [26] V. Forch, T. Franke, N. Rauh, and J. F. Krems, "Are 100 ms fast enough? characterizing latency perception thresholds in mouse-based interaction," in *Engineering Psychology and Cognitive Ergonomics: Cognition and Design*, D. Harris, Ed. Cham: Springer International Publishing, 2017, pp. 45–56.



**Jack T. Hughes** is a Software Engineering major with a minor in Mathematics. His research interests include robotics, embedded software design, software optimization, and autonomous navigation and decision making.



**Garegin Mazmanyan** holds a B.S. in Computer Science from the University of Arizona and is currently pursuing his M.S. in Computer Science at the same institution, specializing in artificial intelligence and robotics. His research focuses on Vision-Language-Action models for autonomous driving, emphasizing transformer-based control and deployment on Quanser's QCar2 platform using ROS2. He has experience in real-time teleoperation, swarm coordination with CrazySwarm2, and VR-based immersive control of aerial and ground robots. His

broader interests include multimodal learning, autonomy pipelines, and the development of safe and reliable robotic systems for real-world applications.



**Mohammad Ghufuran** holds an M.Engg. in Robotics and Automation from the University of Arizona and a B.Tech. in Mechanical Engineering from India. His work focuses on robotics, mechatronics, sensor integration, and autonomous systems. His research experience spans motion planning, human-robot collaboration, and heterogeneous robot coordination. He is passionate about advancing intelligent automation by fusing mechanical design and control systems.



**Hossein Rastgoftar** an Assistant Professor at the University of Arizona. Prior to this, he was an adjunct Assistant Professor at the University of Michigan from 2020 to 2021. He was also an Assistant Research Scientist (2017 to 2020) and a Postdoctoral Researcher (2015 to 2017) in the Aerospace Engineering Department at the University of Michigan Ann Arbor. He received the B.Sc. degree in mechanical engineering-thermo-fluids from Shiraz University, Shiraz, Iran, the M.S. degrees in mechanical systems and solid mechanics from Shiraz University and the University of Central Florida, Orlando, FL, USA, and the Ph.D. degree in mechanical engineering from Drexel University, Philadelphia, in 2015.